RSC Advances

PAPER

View Article Online
View Journal | View Issue

Cite this: *RSC Adv.*, 2023, **13**, 17202

NIR squaraine dyes for dual colorimetric and fluorescent determination of Fe^{3+}, Cu^{2+}, and Hg^{2+} ions†

Huifang Li,‡ Yiru Tang,‡ Kunrong Shen, Ji Lu, Zhijie Zhang, Dong Yi, Na Hao, Qiang Fu, Zi Ye, Jun Wei, Jun Wang, Xianchao Pan, Siping Wei * and Lin Yang *

Four benzoindolenine-based squaraine dyes (SQs), which have the advantages of intense visible and near-infrared (NIR) absorption and emission ($\lambda_{abs/max}$ 663–695 nm, $\lambda_{em/max}$ 686–730 nm) were synthesized and characterized by UV-vis absorption, fluorescent emission spectrophotometry, FTIR, NMR and HRMS analysis. Among them, BBSQ showed excellent performance, which exhibited high selectivity to Fe^{3+}, Cu^{2+}, and Hg^{2+} in acetonitrile solution even in the presence of other competitive metal ions, accompanied by obvious color change easily detected by the naked eye. The detection limit was 14.17 μM for Fe^{3+} and 6.06 μM for Cu^{2+}. Most importantly, the response mechanism of BBSQ to Fe^{3+}, Cu^{2+}, and Hg^{2+} involves the coordination of BBSQ and metal ions through the O atom on the central squarate ring, N atom, and olefin π bond of BBSQ and has been demonstrated by Job's plot, FTIR, and ^{1}H NMR titration analyses. Furthermore, BBSQ was applied successfully to detect Fe^{3+}, Cu^{2+}, and Hg^{2+} in thin-layer chromatography (TLC) plates with good precision and is quite promising for the quantitative detection of Fe^{3+} and Cu^{2+} ions in water samples.

Received 12th April 2023
Accepted 26th May 2023

DOI: 10.1039/d3ra02419a

rsc.li/rsc-advances

1. Introduction

With the development of society and the continuous improvement of human living standards, the accompanying negative problems have become more and more serious, among which the impact of metal ions, anions, and biomolecules on people's daily life and the ecological environment cannot be underestimated.[1] Heavy metals cause great harm to the environment and human life by polluting land and water, which is not conducive to the growth of animals and plants.[2–4] Iron is involved in oxygen transport and proton transfer in blood and is an important component of various enzymes and hemoglobin.[5] The lack of iron in the body will lead to physiological dysfunction, thereby causing diseases. Excess iron is also potentially harmful, becoming toxic by promoting the oxidation of fats, proteins, and other components of the cell.[6] Similarly, the lack or excess of copper ions in the body can lead to growth and metabolic disorders, leading to severe disorders of copper metabolism.[6–8] In addition, mercury is a heavy metal element with high toxicity to human beings and the environment, and its accumulation in the body will lead to serious health problems.[2,3,9,10]

A variety of detection methods have been used to detect metal ions, for example, atomic fluorescence spectrometry (AFS), atomic absorption spectrometry (AAS), inductively coupled plasma (ICP), chemical titration, electrochemical analysis, and chromatography.[7,11] Although these methods have the advantages of low detection limit and high sensitivity, they also have the disadvantages of expensive instruments, complex operation, troublesome pre-processing, and long-time consumption.[4] Therefore, the development of efficient and reliable analytical methods to detect metal ions in real-time is of great significance for food safety problems, early diagnosis of diseases, and environmental level monitoring.[8] Colorimetric and fluorescence detection technology realizes the visual detection of metal ions, simplifies the analysis operation, and improves the detection sensitivity, which plays an important role in promoting the research and solution of problems that plague the origin of human life, disease diagnosis, and treatment, as well as environmental pollution and food safety issues.[5,12] There are a large number of colorimetric and fluorescent metal ion probes with various organic molecular platforms, including boron-dipyrromethene (BODIPY), rhodamine, fluorescein, coumarin, and naphthimide (shown in Table S1†), whose absorption and fluorescence emission wavelength are usually in the ultraviolet and visible (UV-vis) regions.[13,14] In order to expand the application of the metal ion probes in biological systems, chromophores and fluorophores such as

Green Pharmaceutical Technology Key Laboratory of Luzhou City, Central Nervous System Drug Key Laboratory of Sichuan Province, School of Pharmacy, Southwest Medical University, Luzhou 646000, PR China. E-mail: swei1225@swmu.edu.cn; yanglinyjl@swmu.edu.cn

† Electronic supplementary information (ESI) available. See DOI: https://doi.org/10.1039/d3ra02419a

‡ These authors contributed equally.

cyanines, and squaraines (SQs) with near-infrared (NIR) absorption and fluorescence emission properties have attracted more and more attention.

Squaraine dyes, a class of resonance stable squaric acid derivatives with zwitterionic characteristics, contain an electron-deficient central squarate ring (A) connecting the two electron-donating groups (D), forming the intramolecular "donor–acceptor–donor" (D–A–D) structure with a large π-conjugate system.[15,16] Indolenine- and benzoindolenine-based squaraines are one of the common squaraine structures, which have been synthesized and employed as photo-therapeutic agents, optical probes, biological imaging, biomarkers, organic photovoltaic donor materials and so on due to their large π conjugate planar structure and good absorption and emission properties in the NIR region.[17–23] Two benzoindolenine-based squaraines BBSQ and BBSQ-NEt were reported by our group in 2019, and BBSQ-NEt was used as an interfacial layer for efficient polymer solar cells with good performance.[15] In the subsequent preliminary study, we found that BBSQ and BBSQ-NEt responded to metal ions. In fact, there are two oxygen atoms on the central squarate ring of the parent structure of squaraine dyes, which can be directly used as coordination sites with metal ions, leading to significant changes in the colorimetric and fluorescence properties.[24,25] In addition, oxygen atoms can be further replaced and modified by sulfur atoms, nitrogen atoms and so on, which may change the coordination ability with metal ions, adjust their photophysical properties, and obtain probe molecules with different response phenomena.[19,22,26]

In this work, in order to investigate the effect of structural changes on the metal ion response by changing the O atoms, four benzoindolenine-based squaraine dyes with different substituents on the central squarate ring, such as oxygen (BBSQ), monosulfur (BBSQ-S), disulfide (BBSQ-SS), and diethylamine group (BBSQ-NEt) were synthesized using readily available raw materials and simple synthetic routes, as shown in Scheme 1. Four squaraine dyes exhibited strong absorption at 600–750 nm and fluorescence emission at 650–850 nm in the deep-red/near-infrared region. The experimental results showed no significant difference in the response of BBSQ, BBSQ-S, BBSQ-SS, and BBSQ-NEt to metal ions. The best-performing BBSQ was selected to thoroughly study its response to metal ions. BBSQ showed good colorimetric and fluorescence recognition capabilities for Fe^{3+}, Cu^{2+}, and Hg^{2+} with short response time and no interference by other ions.

2. Experimental section

2.1. Reagents

All solvents and reagents (analytical and spectroscopic grades) were obtained commercially and were used as received unless otherwise noted. 1,1,2-Trimethyl-1*H*-benzo[*e*]indole, nitromethane, *n*-butane iodide, squaric acid, quinoline, phosphorus pentasulfide, pyridine, Lawesson's reagent, hexamethylphosphoramide (HMPA), methyl trifluoromethanesulfonate, diethylamine, potassium bromide, metal salts (except for mercury perchlorate and zinc perchlorate, all other salts are chlorides), and all reagents were of analytical or spectral grade purity. The experimental water was ultrapure water.

2.2. Synthesis of target compounds

The synthetic routes are outlined in Scheme 1. B-C4, BBSQ, BBSQ-OMe, BBSQ-NEt, BBSQ-S, and BBSQ-SS were prepared according to the procedures described in the literatures.[15,27]

2.2.1 Synthesis of BBSQ. 1,1,2-Trimethyl-1*H*-benzo[*e*]indole (10.00 g, 47.50 mmol) was added to 80 mL CH_3NO_2, stirred, and dissolved. After adding *n*-butane iodide (21.50 g, 95.50 mmol), the reaction mixture was heated to 100 °C for 14 h, and monitored by thin layer chromatography (TLC). It was detected that some raw materials in the system were still unreacted; thus, 1.80 mL *n*-butane iodide was added, and the reaction mixture was further heated at 100 °C for 4 h. The reaction solution was concentrated to about 50 mL and titrated with 350 mL ethyl acetate. The precipitate was filtered, washed with petroleum

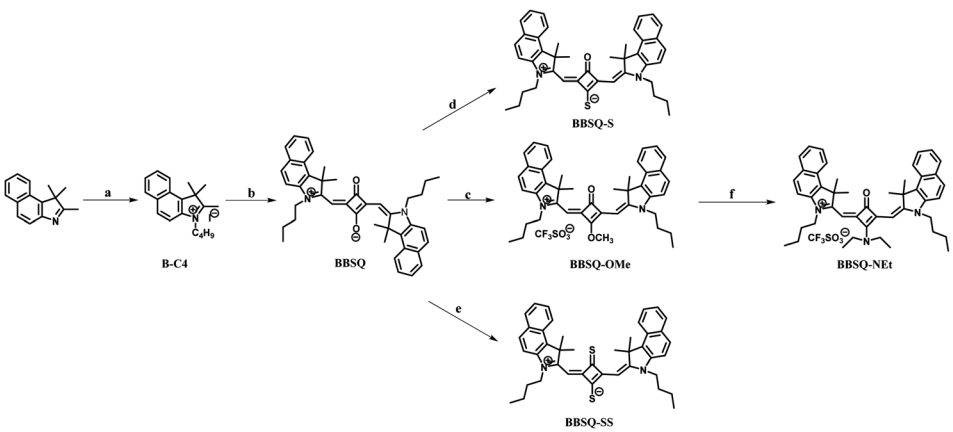

Scheme 1 The synthetic routes of intermediates and target compounds. Reagents/reaction conditions: (a) *n*-butane iodide, nitromethane, 100 °C, 18 h, 86%; (b) squaric acid, quinoline, toluene/*n*-butanol = 1 : 1 (v/v), reflux, 9 h, 54%; (c) methyl trifluoromethanesulfonate, anhydrous dichloromethane, argon, room temperature, 12 h, 49%; (d) phosphorus pentasulfide, pyridine, room temperature, 26 h, 69%; (e) Lawesson's reagent, HMPA, toluene, 115 °C, 2.5 h, 33%; (f) diethylamine, dichloromethane, argon, room temperature, 12 h, 62%.

ether, and then filtered to obtain light gray-green precipitate B-C4 (16.00 g, yield 86%).

B-C4 (10.00 g, 25.4 mmol), squaric acid (1.45 g, 12.7 mmol), quinoline (3.30 g, 25.4 mmol) were added to 150 mL mixed solvent of toluene/*n*-butanol (v/v = 1 : 1). The reaction mixture was refluxed with a Dean–Stark trap for 9 h. The reaction solution was concentrated under reduced pressure to 20 mL and 300 mL of ethyl acetate was added to it. The formed precipitate was suction filtered, washed with 200 mL of petroleum ether twice, and suction filtered to obtain brownish green solid BBSQ (4.16 g, yield 54%). M.p. 302.7–304.1 °C. ^{1}H NMR (400 MHz, chloroform-*d*, ppm) δ 8.20 (d, J = 8.5 Hz, 2H, ArH), 7.90 (d, J = 8.6 Hz, 2H, ArH), 7.87 (d, J = 8.4 Hz, 2H, ArH) 7.58 (t, J = 7.7 Hz, 2H, ArH), 7.42 (t, J = 7.6 Hz, 2H, ArH), 7.29 (d, J = 8.7 Hz, 2H, ArH), 6.03 (s, 2H, =CH), 4.12 (s, 4H, CH_2), 2.09 (s, 12H, CH_3), 1.90–1.83 (m, 4H, CH_2), 1.54–1.46 (m, 4H, CH_2), 1.01 (t, J = 7.4 Hz, 6H, CH_3). ^{13}C NMR (101 MHz, chloroform-*d*, ppm) δ 178.0, 171.4, 139.7, 134.4, 131.2, 129.7, 129.6, 128.7, 127.3, 124.3, 122.6, 110.2, 86.3, 51.2, 43.7, 29.4, 26.8, 20.4, 13.9. HRMS (ESI): *m*/*z* calcd for $[C_{42}H_{44}N_2O_2]^+$ ($[M + H]^+$): 609.3476; found 609.3475.

2.2.2 Synthesis of BBSQ-S. BBSQ (0.54 g, 0.89 mmol) and phosphorus pentasulfide (0.79 g, 1.80 mmol) were reacted in pyridine (6 mL) for 26 h at room temperature. The reaction solution was concentrated and purified by column chromatography with 200–300 mesh of silica gel (eluent: dichloromethane) to obtain a relatively pure product. The product was washed with *n*-hexane to obtain dark green solid BBSQ-S (0.39 g, yield 69%). M.p. 197.7–199.4 °C. ^{1}H NMR (400 MHz, chloroform-*d*, ppm) δ 8.22 (d, J = 8.5 Hz, 2H, ArH), 7.91 (d, J = 6.9 Hz, 2H, ArH), 7.89 (d, J = 7.4 Hz, 2H, ArH), 7.57 (t, J = 7.8 Hz, 2H, ArH), 7.42 (t, J = 7.6 Hz, 2H, ArH), 7.34 (d, J = 8.9 Hz, 2H, ArH), 6.50 (s, 2H, =CH), 4.22 (t, J = 7.5 Hz, 4H, CH_2), 2.11 (s, 12H, CH_3), 1.96–1.85 (m, 4H, CH_2), 1.54–1.47 (m, 4H, CH_2), 1.01 (t, J = 7.5 Hz, 6H, CH_3). ^{13}C NMR (101 MHz, chloroform-*d*, ppm) δ 205.7, 182.7, 177.9, 173.2, 139.6, 134.7, 131.4, 129.8, 129.7, 128.6, 127.4, 124.5, 122.5, 110.4, 88.9, 51.3, 43.8, 29.5, 26.7, 20.4, 14.0. HRMS (ESI): *m*/*z* calcd for $[C_{42}H_{44}N_2OS]^+$ ($[M + H]^+$): 625.3247; found 625.3257.

2.2.3 Synthesis of BBSQ-SS. BBSQ (0.20 g, 0.33 mmol), Lawesson's reagent (0.27 g, 0.66 mmol), and hexamethylphosphoryltriamide (HMPA, 0.13 mL) were added to 15 mL of degassed toluene under anhydrous anaerobic conditions, and the mixture was refluxed for 2.5 h. The reaction solution was added to 100 mL of diethyl ether to form a precipitate. The solid was dissolved in dichloromethane, purified by column chromatography with 200–300 mesh of silica gel (eluent: dichloromethane/petroleum ether = 1 : 1, v/v), and recrystallized (dichloromethane : ethanol = 1 : 3, v/v) to obtain bright copper solid BBSQ-SS (0.07 g, yield 33%). M.p. 242.2–243.6 °C. ^{1}H NMR (400 MHz, chloroform-*d*, ppm) δ 8.21 (d, J = 8.5 Hz, 2H, ArH), 7.92 (d, J = 8.0 Hz, 2H, ArH), 7.90 (d, J = 8.5 Hz, 2H, ArH), 7.59 (t, J = 7.7 Hz, 2H, ArH), 7.45 (t, J = 7.6 Hz, 2H, ArH), 7.37 (d, J = 8.0 Hz, 2H, ArH), 6.63 (s, 2H, =CH), 4.36 (t, J = 7.6 Hz, 4H, CH_2), 2.14 (s, 12H, CH_3), 1.93–1.86 (m, 4H, CH_2), 1.56–1.46 (m, 4H, CH_2), 1.02 (t, J = 6.0 Hz, 6H, CH_3). ^{13}C NMR (101 MHz, chloroform-*d*, ppm) δ 204.5, 185.1, 174.9, 139.4, 135.0, 131.4, 129.7, 129.6, 128.6, 127.3, 124.6, 122.7, 110.7, 87.5, 51.6, 45.2, 29.4, 27.6, 20.3, 13.9. HRMS (ESI): *m*/*z* calcd for $[C_{42}H_{44}N_2S_2]^+$ ($[M + Na]^+$): 663.2838; found 663.2836.

2.2.4 Synthesis of BBSQ-NEt. BBSQ (3.00 g, 4.93 mmol) and $CF_3SO_3CH_3$ (4.04 g, 24.64 mmol) were added to 90 mL of degassed anhydrous dichloromethane, and the reaction mixture was stirred at room temperature under argon protection for 12 h and poured into water. The organic phase was separated and the aqueous phase was extracted with CH_2Cl_2 three times. The combined organic phase was dried over anhydrous Na_2SO_4, filtered, and concentrated *in vacuo* to obtain yellow-green solid BBSQ-OMe.

BBSQ-OMe (0.40 g, 0.52 mmol) and diethylamine (0.19 g, 2.59 mmol) were added to 50 mL degassed anhydrous dichloromethane. The mixture was reacted at room temperature for 12 h under argon protection, then concentrated, purified by column chromatography with 200–300 mesh of neutral alumina (eluent: dichloromethane/methanol = 60 : 1, v/v), and recrystallized (dichloromethane : *n*-hexane) to obtain brown metallic-luster needle-like crystals of BBSQ-NEt (0.26 g, yield 62%). M.p. 203.2–204.7 °C. ^{1}H NMR (400 MHz, chloroform-*d*, ppm) δ 8.16 (d, J = 8.5 Hz, 2H, ArH), 7.95 (d, J = 4.0 Hz, 2H, ArH), 7.93 (d, J = 4.0 Hz, 2H, ArH) 7.61 (t, J = 8.0 Hz, 2H, ArH), 7.49 (t, J = 7.5 Hz, 2H, ArH), 7.41 (d, J = 8.8 Hz, 2H, ArH), 5.86 (s, 2H, =CH), 4.27 (t, J = 7.4 Hz, 4H, CH_2), 3.94 (q, J = 8.0 Hz, 4H, CH_2), 2.00 (s, 12H, CH_3), 1.87–1.79 (m, 4H, CH_2), 1.58 (t, J = 7.1 Hz, 6H, CH_3), 1.48–1.41 (m, 4H, CH_2), 0.98 (t, J = 7.3 Hz, 6H, CH_3). ^{13}C NMR (101 MHz, chloroform-*d*, ppm) δ 173.7, 173.5, 165.2, 157.3, 138.1, 134.0, 130.9, 129.2, 128.9, 127.3, 126.6, 124.1, 121.5, 110.0, 86.5, 50.9, 46.0, 44.5, 28.7, 25.3, 19.3, 14.4, 12.9. ^{19}F NMR (376 MHz, chloroform-*d*, ppm) δ −78.07. HRMS (ESI): *m*/*z* calcd for $[C_{47}H_{54}F_3N_3O_4S]^+$ ($[M]^+$): 813.3787; found 813.3777.

2.3. Spectral test conditions

UV-vis absorption spectra were recorded using a Shimadzu UV-3600 Plus atomic absorption spectrophotometer. Fluorescence emission spectra were recorded on the FS5 fluorescence spectrophotometer at the excitation wavelength of 620 nm with an excitation slit width of 5 nm and an emission slit width of 1 nm. Stock solutions of the probe molecules (2.0 mM) were prepared in dichloromethane. Test probe solutions (10 μM) were prepared by placing 50 μL of probe stock solution into a test tube and diluted to 10 mL with CH_3CN. Stock solutions of various metal ions (40 mM, Fe^{3+}, Cu^{2+}, Hg^{2+}, Fe^{2+}, Na^+, K^+, Li^+, Ca^{2+}, Ba^{2+}, Al^{3+}, Pb^{2+}, Mn^{2+}, Co^{2+}, Zn^{2+}, Ag^+, Mg^{2+}, Ni^{2+}, Cd^{2+}, Cr^{3+}, and Cr^{2+}) were prepared in deionized water. In the titration experiments, test solutions were prepared with 10 μM BBSQ acetonitrile solutions with different concentrations of Fe^{3+}, Cu^{2+}, and Hg^{2+}, respectively. The detection limit formula is LOD = $3\delta/k$; δ is the standard deviation of the blank solution; k is the slope of the calibration curve. In selectivity experiments, the test samples were prepared by placing appropriate amounts of the cations stock solutions (40 mM) into 10 mL of BBSQ, BBSQ-S, BBSQ-SS, and BBSQ-NEt acetonitrile solution (10 μM). For the interference test, the test samples were prepared by adding 50

μL of other metal ion stock solutions into BBSQ acetonitrile solution (10 μM) containing Fe^{3+} (20 equiv.), Cu^{2+} (20 equiv.) and Hg^{2+} (20 equiv.). For the response time test, the test samples were 10 μM BBSQ acetonitrile solution containing Fe^{3+} (12 equiv.), Cu^{2+} (4 equiv.), and Hg^{2+} (4 equiv.) respectively, and the change in the fluorescence emission intensity of the BBSQ probe at 686 nm was measured as a function of the reaction time. In Job's plot curve experiments, the test samples containing BBSQ and Fe^{3+}, Cu^{2+}, and Hg^{2+}, the total concentration of BBSQ and metal ions was maintained at 10 μM. The molar fractions of Fe^{3+}, Cu^{2+}, and Hg^{2+} were taken at equal intervals between 0–1, and the fluorescence emission intensity of the samples at 686 nm was tested after a period of reaction.

^{1}H NMR and ^{13}C NMR spectra were recorded on a Bruker AscendTM 400 MHz Superconducting Nuclear Magnetic Resonance Spectrometer using a deuterated solvent as the lock and TMS as an internal reference. For ^{1}H NMR titration of BBSQ with Fe^{3+}, Cu^{2+}, and Hg^{2+}, BBSQ (18 mM in $CDCl_3$) was titrated by adding known quantities of metal ions salts. High-resolution mass spectra (HRMS) were recorded on Waters G2-XS QTOf and Shimadzu LCMSIT-TOF instruments. FTIR spectra were recorded on an IRAffinity-1S Fourier Transform Infrared Spectrophotometer (KBr pellet method). The melting points were recorded using an MP470 Automatic Video Melting Point Meter.

3. Results and discussion

3.1. Photophysical properties of BBSQ, BBSQ-S, BBSQ-SS, and BBSQ-NEt

To verify the efficacy of solvent, the response of BBSQ to various metal ions in CH_3CN, DMSO, MeOH, and H_2O was studied (Fig. S1–S4†). BBSQ was insoluble in H_2O. The DMSO system of BBSQ did not respond to metal ions, while the CH_3CN system of BBSQ responded to Fe^{3+}, Cu^{2+}, and Hg^{2+} ions and the MeOH system of BBSQ responded to Fe^{3+}, Cu^{2+}, and Ag^{+} ions. The experimental results show that different solvents can affect the interactions between BBSQ and each metal ion, thus affecting the selectivity of BBSQ for metal ions. Additionally, the UV-vis absorption spectra of BBSQ with the concentration of 0–16 μM in CH_3CN were recorded. As depicted in Fig. S5,† a good linear correlation could be obtained between the concentration of BBSQ and the absorbance value at 663 nm, indicating that the BBSQ showed good solubility in CH_3CN in the concentration range of 1–16 μM. Therefore, BBSQ CH_3CN (10 μM) system should be suitable for this study.

The UV-vis absorption spectra and fluorescence emission spectra of BBSQ, BBSQ-S, BBSQ-SS, and BBSQ-NEt in acetonitrile solution were analysed. As shown in Fig. 1 and Table 1, all four probe molecules exhibited sharp and strong absorption peaks in the near-infrared region with the maximum absorption wavelengths ($\lambda_{abs/max}$) located at 663, 668, 679, and 695 nm for BBSQ, BBSQ-S, BBSQ-SS, and BBSQ-NEt, respectively. Meanwhile, they showed red-shifted emission spectra with the corresponding maximum emission wavelength located at 686, 694, 704, and 730 nm. Obviously, as the oxygen atoms on the central squarate ring were replaced with monosulfur atoms, disulfide atoms, and diethylamine group, the absorption and emission

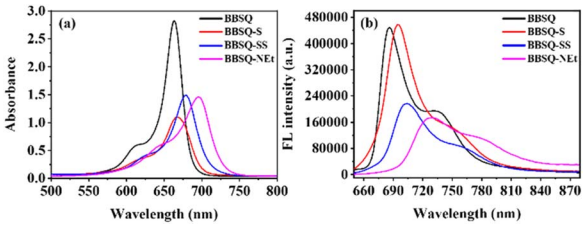

Fig. 1 (a) UV-vis absorption spectra and (b) fluorescence emission spectra of the four probe molecules.

Table 1 Spectral properties and ion-responsive properties of the four compounds

	$\lambda_{abs/max}$ [nm]	$\lambda_{em/max}$ [nm]	Response to ions	LOD (Fe^{3+}) [μM]
BBSQ	663	686	Fe^{3+}, Hg^{2+}, Cu^{2+}	14.17
BBSQ-S	668	694	Fe^{3+}, Hg^{2+}, Cu^{2+}	32.81
BBSQ-SS	679	704	Fe^{3+}, Hg^{2+}, Cu^{2+}	41.73
BBSQ-NEt	695	730	Fe^{3+}, Hg^{2+}, Cu^{2+}	46.32

spectra of the probe molecules showed a significant red shift, which is consistent with the results reported in the literature.[27–29] Simultaneously, the ^{1}H NMR spectra analysis showed that the methane protons were seen at δ 6.03 ppm for BBSQ, where the same signal moved proportionally to the lower field at δ 6.50 ppm and 6.63 ppm for monothiosquaraine BBSQ-S and dithiosquaraine BBSQ-SS, respectively, while the same signal of BBSQ-NEt with diethylamine group moved towards the higher field at δ 5.86 ppm. These results show that the changes of oxygen atoms on the central squarate ring will affect the electronic distribution and photophysical properties of these probe molecules.

3.2. Selectivity study of BBSQ, BBSQ-S, BBSQ-SS, and BBSQ-NEt to various metal ions

In order to explore the selective response of these four probe molecules to metal ions, UV-vis absorption and fluorescence emission spectra of BBSQ, BBSQ-S, BBSQ-SS, and BBSQ-NEt were recorded in the presence of a variety of metal ions (Fe^{3+}, Cu^{2+}, Hg^{2+}, Fe^{2+}, Na^{+}, K^{+}, Li^{+}, Ca^{2+}, Ba^{2+}, Al^{3+}, Pb^{2+}, Mn^{2+}, Co^{2+}, Zn^{2+}, Ag^{+}, Mg^{2+}, Ni^{2+}, Cd^{2+}, Cr^{3+}, and Cr^{2+}), shown in Fig. 2, S4, S6–S8,† and Table 1. It can be found that the colour of the BBSQ CH_3CN solution changed from blue to yellow after Fe^{3+}, Cu^{2+}, and Hg^{2+} were added; accordingly, the absorbance of BBSQ at 663 nm and the fluorescence emission intensity at 686 nm significantly decreased to about 0. However, when other metal ions were added, the colour, absorbance, and fluorescence intensity did not show obvious changes. For BBSQ-S, BBSQ-SS, and BBSQ-NEt, their response to these metal ions is relatively similar to BBSQ, all selectively responding to Fe^{3+}, Cu^{2+}, and Hg^{2+}. Although Fe^{2+} ion caused a color change in the BBSQ solution (Fig. 2a and S4†), Fe^{2+} ion did not induce an obvious response in the fluorescence spectrum. Ag^{+} ion and BBSQ-SS showed a similar situation (Fig. 2c and S7†). As such, Fe^{2+} and Ag^{+} were not discussed when studying the colorimetric and

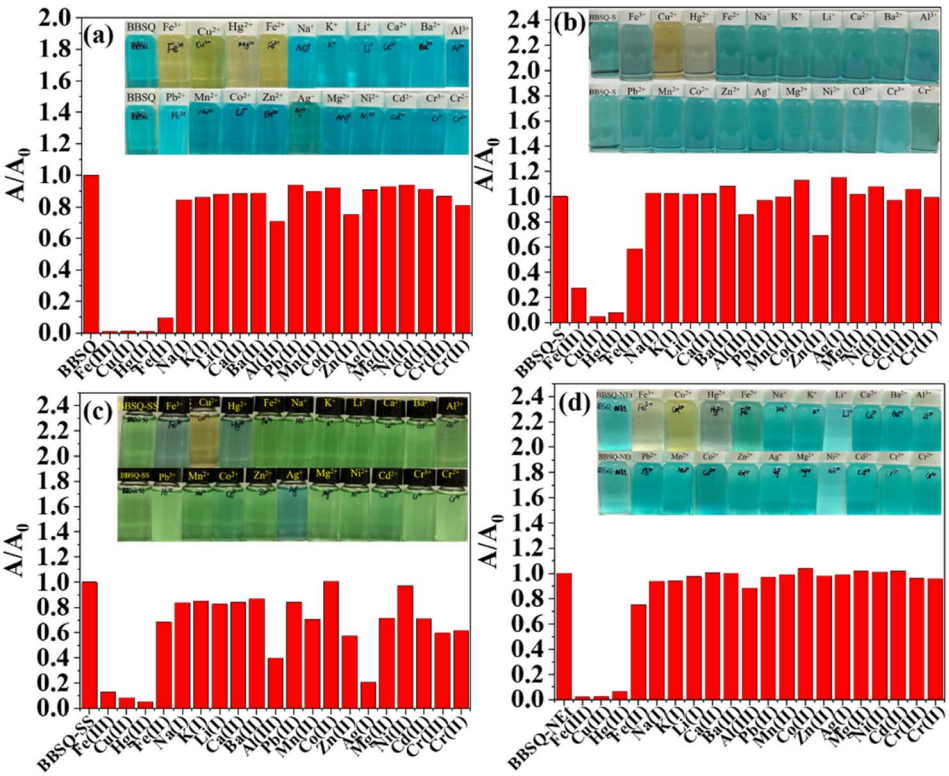

Fig. 2 UV-vis absorption spectra selective histogram and colorimetric photographs of (a) BBSQ (10 μM), (b) BBSQ-S (10 μM), (c) BBSQ-SS (10 μM), and (d) BBSQ-NEt (10 μM) acetonitrile solution with different metal ions (20 equiv.).

fluorescent dual response of these probes to metal ions.[30] The above results indicate that the change of oxygen atoms on the central squarate ring of BBSQ did not significantly affect their selective response to metal ions. However, compared with BBSQ-S, BBSQ-SS, and BBSQ-NEt, the absorbance and fluorescence intensity of BBSQ in response to Fe^{3+}, Cu^{2+}, and Hg^{2+} were quenched more thoroughly, and the colour change of the solution was also more obvious. Concurrently, the detection limit of Fe^{3+} was obtained by the concentration titration experiments of four probe molecules, and BBSQ showed the lowest detection limit of Fe^{3+} with 14.17 μM by the absorption of spectral titration. Therefore, BBSQ was selected as a representative probe molecule to further investigate the detection effect and response mechanism to Fe^{3+}, Cu^{2+}, and Hg^{2+}.

3.3. Anti-interference study of BBSQ in response to Fe^{3+}, Cu^{2+}, and Hg^{2+}

The results of the selectivity experiments indicate a favourable selective response of BBSQ to Fe^{3+}, Cu^{2+}, and Hg^{2+}. In order to further explore the interference effects of other metal ions, the absorption and fluorescence responses of BBSQ (10 μM) to competitive metal ions were analysed. As shown in Fig. 3 and S9–S11,† when Fe^{3+}, Cu^{2+}, and Hg^{2+} (20 equiv.) were added, the absorbance of BBSQ acetonitrile solution at 663 nm decreased sharply to almost disappear, and when other interfering metal ions (20 equiv.) were later added, the absorbance of the system showed no significant variation. Similarly, no substantial change in the fluorescence spectra was observed when BBSQ responded to Fe^{3+}, Cu^{2+}, and Hg^{2+} in the presence of other metal

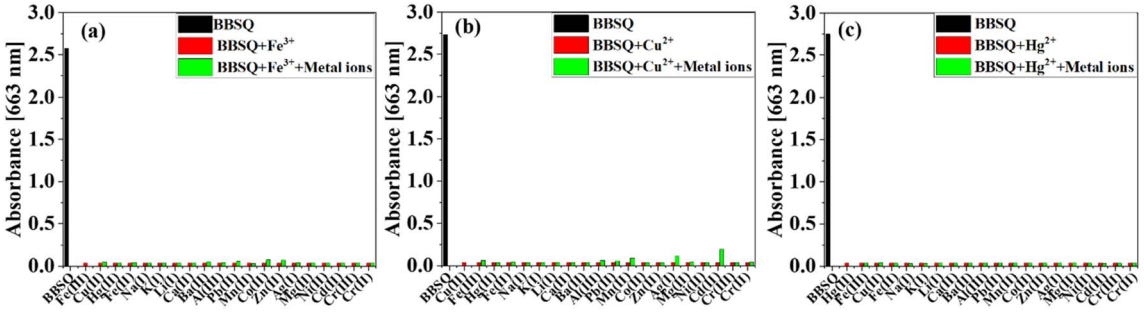

Fig. 3 Absorption intensity at 663 nm of BBSQ (10 μM) in the presence of (a) Fe^{3+} (20 equiv.), (b) Cu^{2+} (20 equiv.), and (c) Hg^{2+} (20 equiv.) along with other metal ions (20 equiv.).

ions. The interference experiments demonstrated the good selective recognition of BBSQ to Fe^{3+}, Cu^{2+}, and Hg^{2+} even in the presence of other metal ions.[1,5]

3.4. UV-vis absorption and fluorescence spectral titrations of BBSQ with Fe^{3+}, Cu^{2+}, and Hg^{2+}

Fig. 4, S12 and S13† show the UV-vis absorption and fluorescence emission spectra of BBSQ (10 μM) in response to different concentrations of Fe^{3+}, Cu^{2+}, and Hg^{2+}. As shown in Fig. 4, BBSQ exhibited a sharp and strong absorption peak at 663 nm. As the concentration of Fe^{3+} increased from 0 μM to 120 μM, the intensity of the absorption peak at 663 nm gradually decreased until almost disappeared, and from 120 μM to 200 μM, the intensity remained unchanged. In addition, the fluorescence emission intensity of BBSQ at 686 nm also gradually weakened with increasing Fe^{3+} concentration from 0 μM to 120 μM and reached saturation from 120 μM to 200 μM. The insets in Fig. 4 show the concentration titration curves with the Fe^{3+} concentration in the abscissa and the absorbance (663 nm) or fluorescence emission intensity (686 nm) as the ordinate. The UV-vis absorption response of BBSQ to Fe^{3+} exhibited a linear correlation within the Fe^{3+} concentration in the range of 15–55 μM, while the fluorescence response of BBSQ to Fe^{3+} exhibited a linear relationship with the Fe^{3+} concentration in the range of 15–95 μM. According to the linear fitting equation and detection limit calculation formula,[31] the detection limit (LOD) of BBSQ toward Fe^{3+} by absorption and fluorescence spectral titration was calculated to be 14.17 μM and 51.7 μM, respectively.

As shown in Fig. S12,† the UV-vis absorption and fluorescence emission spectra of BBSQ (10 μM) in response to different concentrations of Cu^{2+} were measured. The absorption peak at 663 nm and fluorescence emission peak at 686 nm of BBSQ gradually decreased with the increase of Cu^{2+} concentration from 0–40 μM. When the Cu^{2+} concentration was 40 μM, the response of BBSQ to Cu^{2+} reached a saturated state. According to the corresponding concentration titration curves, the LOD of BBSQ toward Cu^{2+} by absorption and fluorescence spectral titration was calculated to be 6.06 μM and 14.17 μM, respectively.

As shown in Fig. S13,† the intensity of the absorption peak at 663 nm and fluorescence emission peak at 686 nm of BBSQ decreased sharply with the gradual increase of Hg^{2+} concentration from 0 μM to 40 μM, and is not linearly correlated. The response of BBSQ to Hg^{2+} reached saturation at 40 μM.

3.5. Response time of BBSQ towards Fe^{3+}, Cu^{2+}, and Hg^{2+}

After adding Fe^{3+} (12 equiv.), Cu^{2+} (4 equiv.) and Hg^{2+} (4 equiv.), the absorption and emission spectra of the BBSQ (10 μM) system were tested immediately and subsequently every 2 min. As shown in Fig. 5, after adding Fe^{3+}, the fluorescence emission

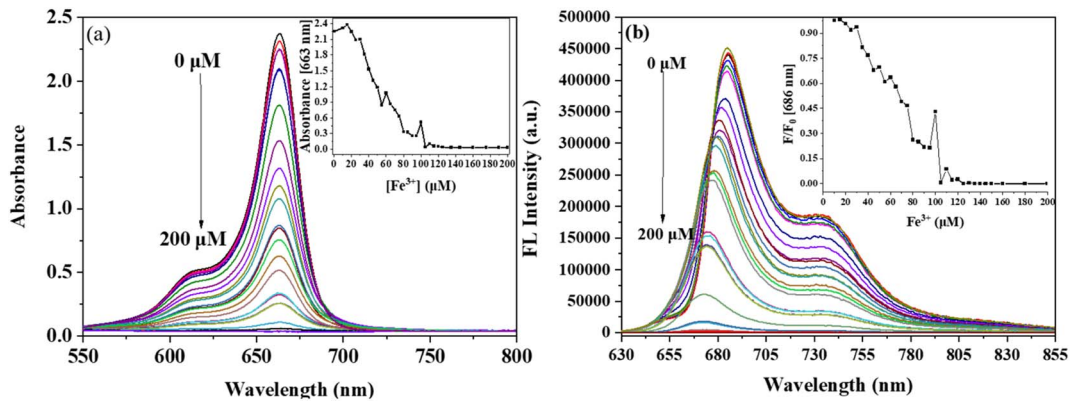

Fig. 4 (a) UV-vis absorption and (b) fluorescence spectral titrations of BBSQ acetonitrile solution (10 μM) with Fe^{3+} (0–200 μM); inset: (a) the concentration titration curves of absorbance at 663 nm and (b) fluorescence emission intensity at 686 nm with increasing Fe^{3+} concentration.

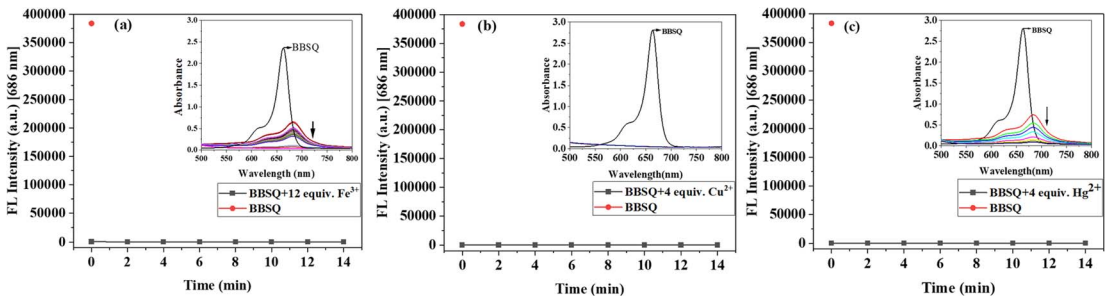

Fig. 5 Time-resolved fluorescence emission pattern and UV-vis absorption spectra (inset) of BBSQ acetonitrile solution with (a) Fe^{3+} (12 equiv.), (b) Cu^{2+} (4 equiv.), and (c) Hg^{2+} (4 equiv.).

intensity at 686 nm of BBSQ was reduced to almost disappear rapidly within a few seconds, followed by no change after 2 min over time. Simultaneously, the absorbance at 663 nm immediately decreased to about 1/3 times, and it gradually decreased over time, reaching equilibrium at about 10 min. The results of the BBSQ response to Hg^{2+} over time were similar to that of Fe^{3+}. For Cu^{2+}, both the fluorescence emission intensity at 686 nm and the absorbance at 663 nm of BBSQ were reduced to almost disappear immediately within a few seconds. The experimental results show that BBSQ can respond to Fe^{3+}, Cu^{2+}, and Hg^{2+} rapidly within a few seconds and complete the detection in about 2 min.

3.6. Response mechanism of BBSQ to Fe^{3+}, Cu^{2+}, and Hg^{2+}

In general, the selectivity of the probe molecules for metal ions depends on the binding ability of the ligands with lone pair electrons such as N, O, and S in their structures to metal ions. Therefore, in order to explore the interaction between BBSQ and Fe^{3+}, Cu^{2+}, and Hg^{2+}, the metal chelator ethylene diamine tetraacetic acid (EDTA) was added to the system after BBSQ responded to Fe^{3+}, Cu^{2+}, and Hg^{2+}, and the corresponding absorption spectra are shown in Fig. 6. After the response of BBSQ to Fe^{3+} or Hg^{2+}, the absorbance at 663 nm decreased sharply, and then after adding EDTA, the reduced absorbance was almost recovered to the metal-free state. However, when BBSQ responded to Cu^{2+} and EDTA was added, the absorbance of the system was not restored quickly and a new absorption peak appeared at 732 nm. These results suggest that the BBSQ responds with Fe^{3+}, Cu^{2+}, and Hg^{2+} through complexation interactions, and the complexation ability of BBSQ–Fe^{3+}, BBSQ–Cu^{2+}, and BBSQ–Hg^{2+} is weaker than that of EDTA-Fe^{3+}, EDTA-Cu^{2+}, and EDTA-Hg^{2+}, respectively.[32,33] Moreover, the different colours caused by the absorption change of BBSQ–metal ion systems after adding EDTA enable the human eye to distinguish Cu^{2+} from Fe^{3+}/Cu^{2+}/Hg^{2+}.

In order to determine the binding ratio of BBSQ–Fe^{3+}, BBSQ–Cu^{2+}, and BBSQ–Hg^{2+}, the Job's plots were collected as shown in Fig. 7. The plots were prepared by recording the fluorescence emission intensity at 686 nm against $[Fe^{3+}]/[Fe^{3+}$ + BBSQ], $[Cu^{2+}]/[Cu^{2+}$ + BBSQ], or $[Hg^{2+}]/[Hg^{2+}$ + BBSQ]. For these three systems, when the molar fraction of Fe^{3+}, Cu^{2+}, and Hg^{2+} approached 0.5, the curve appeared at an inflection point, indicating that the binding ratio of probe BBSQ to Fe^{3+}, Cu^{2+}, and Hg^{2+} was 1 : 1,[9,32] which was also confirmed from the ESI-HRMS data (shown in Fig. S28–S30†). A solution containing BBSQ with 1 equiv. of $FeCl_3$ showed a strong peak at 769.17, assigned to [BBSQ–$FeCl_3^+$] ion,[34] while the BBSQ–Cu^{2+} system showed a peak at 671.3481, assigned to [BBSQ–Cu^{2+}], and BBSQ–Hg^{2+} system showed a peak at 945.6797, assigned to [BBSQ–Hg^{2+} + $2CH_3CN$ + $2H_2O$ + OH^-].

In order to further investigate the binding properties of BBSQ with Fe^{3+}, Cu^{2+}, and Hg^{2+}, ^{1}H NMR and FT-IR spectra of BBSQ, BBSQ–Fe^{3+}, BBSQ–Cu^{2+}, and BBSQ–Hg^{2+} were tested. As shown in Fig. 8,[10] BBSQ showed a single peak of olefin proton (H_a) at 6.03 ppm, and a broad peak of methylene proton (H_b) at 4.11 ppm. With the addition of 0.1 equiv. Fe^{3+}, Cu^{2+}, or Hg^{2+} to BBSQ CD_3CN solution, the multiple signals of aromatic and aliphatic protons broadened due to the paramagnetic nature of

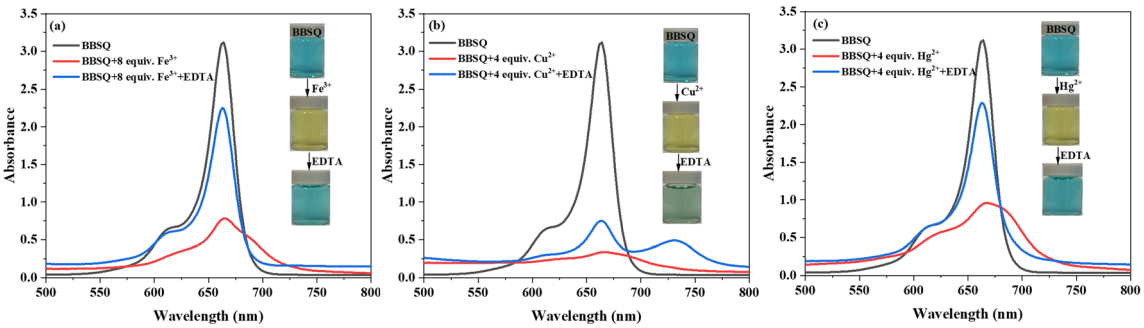

Fig. 6 UV-vis absorption spectra of BBSQ and BBSQ in response to (a) Fe^{3+} (8 equiv.), (b) Cu^{2+} (4 equiv.), (c) Hg^{2+} (4 equiv.) with/without adding EDTA.

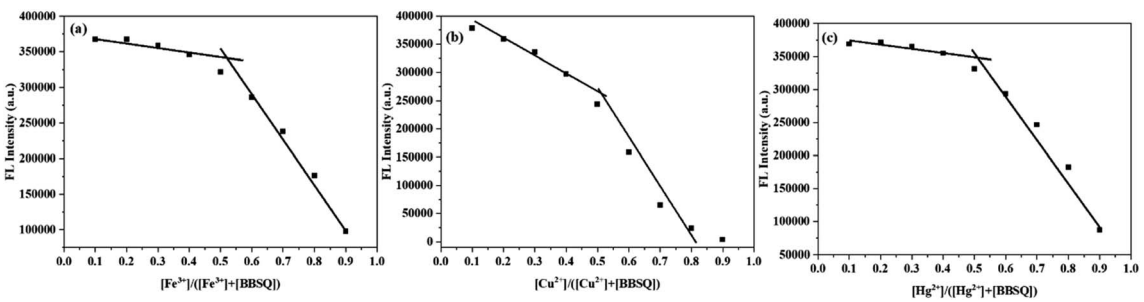

Fig. 7 Job's plots of interaction between (a) Fe^{3+} and BBSQ, (b) Cu^{2+} and BBSQ, and (c) Hg^{2+} and BBSQ.

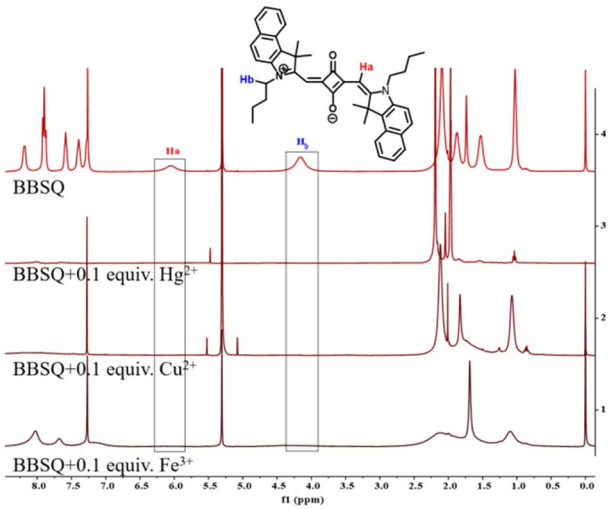

Fig. 8 ^{1}H NMR spectra of BBSQ and with 0.1 equiv. Fe^{3+}/Cu^{2+}/Hg^{2+} in CD_3CN (10 mM).

the Fe^{3+}, Cu^{2+}, and Hg^{2+} metal ions; moreover, the signal intensity of H_a at 6.03 ppm and H_b at 4.11 ppm decreased to nearly vanish, indicating that BBSQ were complexed with Fe^{3+}, Cu^{2+}, and Hg^{2+} through the N atom and olefin π bond.[35] Olefins with π bonds can also be used as ligands, which are called π bond ligands.[35]

As shown in Fig. 9, BBSQ exhibited a strong peak at 1576 cm^{-1} in the FTIR spectrum, which corresponded to the C=C stretching vibration of the central squarate ring.[36] However, for BBSQ–Fe^{3+}, BBSQ–Cu^{2+}, and BBSQ–Hg^{2+} systems, the characteristic peak of BBSQ at 1576 cm^{-1} shifted to 1628 cm^{-1}, and C=O stretching peak was observed at 1739 cm^{-1} even in BBSQ–Fe^{3+} systems, which indicates that O atom on the central squarate ring of BBSQ was involved in the recognition of these three metal ions.[10] Simultaneously, the tensile vibration peak of N–C in the range of 1216–1310 cm^{-1} and the C–H vibration peak at 851 cm^{-1} of the alkenyl group near the central squarate ring also changed significantly compared to those of BBSQ. The result assures that Fe^{3+}, Cu^{2+},

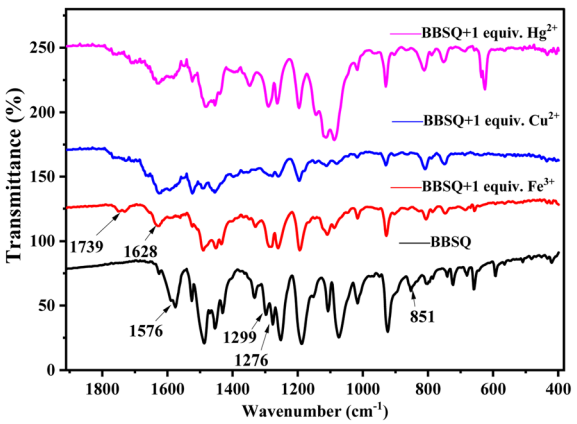

Fig. 9 FTIR spectra of BBSQ and with 1 equiv. Fe^{3+}, Cu^{2+}, and Hg^{2+}.

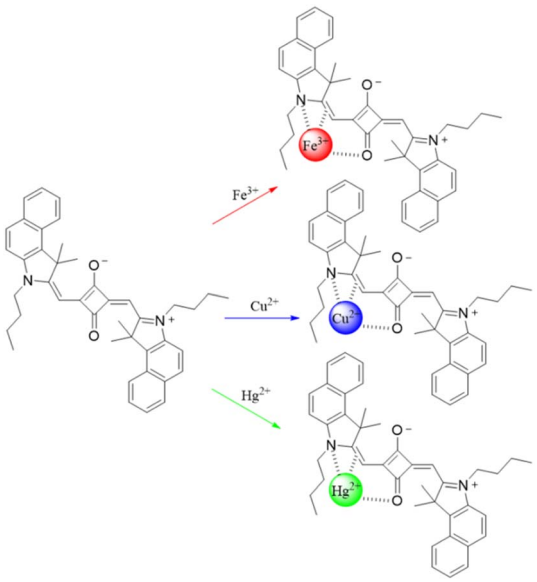

Fig. 10 The proposed chelating mechanism of BBSQ with Fe^{3+}, Cu^{2+}, and Hg^{2+}.

and Hg^{2+} bond with the O atom, N atom, and olefin π bond of BBSQ, which is consistent with the results of ^{1}H NMR measurement. Therefore, the specific response of BBSQ to Fe^{3+}, Cu^{2+} and Hg^{2+} ions might be attributed to the strong coordination ability of transition metal Fe^{3+}, Cu^{2+}, and Hg^{2+} ions. Moreover, among transition metal ions, Fe^{3+}, Cu^{2+}, and Hg^{2+} have higher electronegativity, which leads to thermodynamically stable complexes in the presence of electron-rich O, N, and olefin π bonds.[37] Hence, according to the results of Job's plot curve, ^{1}H NMR and FTIR spectra, and the relevant references,[10,35,36] the proposed chelating mechanism of BBSQ with Fe^{3+}, Cu^{2+}, and Hg^{2+} metal ions is depicted in Fig. 10.

3.7. Practical application of BBSQ

The detection parameters of BBSQ and some reported probes for Fe^{3+}, Cu^{2+}, and Hg^{2+} are summarized in Table S1.† Compared with the other probes, BBSQ shows a relatively high detection limit, and the sensitivity needs further improvement. However, BBSQ also shows the advantages of NIR detection wavelength, fast response time in a few seconds, and the

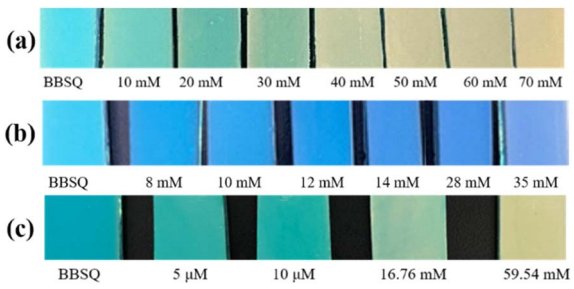

Fig. 11 Photographs of the BBSQ-loaded TLC plates before and after (a) Fe^{3+}, (b) Cu^{2+}, and (c) Hg^{2+} processing.

Table 2 BBSQ detection of Fe^{3+} and Cu^{2+} in real water samples

Sample	Metal ion	Spiked (μM)	Recovered (μM)	Recovery (%)
Yudaihe River	Fe^{3+}	0	Not detected	—
		20	18.73 ± 0.01	94
		30	32.44 ± 0.06	108
	Cu^{2+}	0	Not detected	—
		20	21.30 ± 1.05	104
		30	28.30 ± 1.90	94

visualization of naked eye detection. Motivated by the advantages, BBSQ loaded on TLC plates were prepared to detect Fe^{3+}, Cu^{2+}, and Hg^{2+} easily and quickly. The TLC plates were immersed in an ethanol solution containing BBSQ (1.92 mM) and dried in air. The TLC plates loaded with BBSQ were immersed in the various concentrations of Fe^{3+}, Cu^{2+}, and Hg^{2+} aqueous solution, then dried in air. Clear visual colour changes of TLC plates were observed to achieve the purpose of detection.[11] As shown in Fig. 11, when detecting Fe^{3+} and Hg^{2+}, the colour of the TLC plates changed gradually from blue to yellow with the increased concentration of Fe^{3+} and Hg^{2+}, and the obvious change in colour was recognized by the naked eye at the concentration of 30 mM for Fe^{3+} and 16.76 mM for Hg^{2+}. For Cu^{2+}, the colour of the TLC plates gradually changed from blue to blue-purple, then constantly deepened to purple. These results show that the simple colorimetric TLC plates loaded with BBSQ can detect Fe^{3+}, Cu^{2+}, and Hg^{2+} by the naked eye quickly and conveniently *in situ*, which is important for practical applications.[38]

In addition, BBSQ was also used to detect Fe^{3+} and Cu^{2+} ions in the water samples from the Yudaihe River in Luzhou city with the standard addition method.[39,40] Since the response of BBSQ to Hg^{2+} ion was not linearly correlated with the concentration of Hg^{2+} ion, the detection of Hg^{2+} ion was not tested. As depicted in Table 2, the pristine water sample could not induce a significant optical response of BBSQ. The different concentrations of Fe^{3+} (20 μM and 30 μM) and Cu^{2+} (20 μM and 30 μM) were spiked into water samples and measured with BBSQ. The results show that Fe^{3+} and Cu^{2+} ions in the water samples could be accurately measured with good recovery (94–108%), indicating that BBSQ is quite promising for the quantitative detection of Fe^{3+} and Cu^{2+} ions in real water samples.[31,41]

4. Conclusion

In summary, four inexpensive and highly selective chemical sensors (BBSQ, BBSQ-S, BBSQ-SS, and BBSQ-NEt) based on benzoindolenine–squaraine dyes were developed. They exhibited strong absorption and emission in the visible and near-infrared regions and showed significant selectivity in the recognition of Fe^{3+}, Cu^{2+}, and Hg^{2+} over other metal ions with obvious colorimetric and fluorescence changes. The stoichiometry of the complex between BBSQ and Fe^{3+}, Cu^{2+}, and Hg^{2+} was revealed in a 1 : 1 composition. ^{1}H NMR titration and FTIR studies proved that Fe^{3+}, Cu^{2+}, and Hg^{2+} are complexed with the O atom on the central squarate ring, N atom, and olefin π bond of BBSQ. Moreover, the BBSQ-loaded TLC plates can detect Fe^{3+}, Cu^{2+}, and Hg^{2+} quickly and conveniently, and BBSQ is quite promising for the quantitative detection of Fe^{3+} and Cu^{2+} ions in real water samples.

Author contributions

Huifang Li: conceptualization, formal analysis, validation, investigation, methodology, writing – original draft. Yiru Tang: validation, investigation. Kunrong Shen: validation. Ji Lu: resources, writing – review, and editing. Zhijie Zhang: resources, writing – review, and editing. Dong Yi: resources, writing – review, and editing. Na Hao: resources, writing – review, and editing. Qiang Fu: investigation, resources, writing – review, and editing. Zi Ye: investigation. Jun Wei: resources, writing – review, and editing. Jun Wang: resources, writing – review, and editing. Xianchao Pan: resources, writing – review, and editing. Siping Wei: resources, writing – review and editing, funding acquisition. Lin Yang: conceptualization, resources, writing – review and editing, funding acquisition, Supervision.

Conflicts of interest

There are no conflicts to declare.

Acknowledgements

We acknowledge the financial support for this work from the Natural Science Foundation of Sichuan Province (2022NSFSC1468 and 2021YJ0226), the Science and Technology Strategic Cooperation Programs of Luzhou Municipal People's Government and Southwest Medical University (2019LZXNYDZ09) and Innovation and Entrepreneurship Training Program for College Students (S202210632137). We are grateful to Drug Analysis and Testing Center, School of Pharmacy, Southwest Medical University for providing NMR and FTIR analyses. We are also grateful to the Public Platform of Advanced Detecting Instruments, Public Center of Experimental Technology, Southwest Medical University for providing the UV-vis absorption and fluorescence spectra measurements.

References

1 Y. Li, Q. Niu, T. Wei and T. Li, *Anal. Chim. Acta*, 2019, **1049**, 196–212.
2 V. Juvekar, S. J. Park, J. Yoon and H. M. Kim, *Coord. Chem. Rev.*, 2021, **427**, 213574.
3 K. Kala and N. Manoj, *RSC Adv.*, 2016, **6**, 22615–22619.
4 D. T. Quang and J. S. Kim, *Chem. Rev.*, 2010, **110**, 6280–6301.
5 D. Zhang, Y. Qi, Y. Li, Y. Song, C. Xian, H. Li and P. Cong, *J. Fluoresc.*, 2021, **31**, 1133–1141.
6 D. Wu, L. Chen, W. Lee, G. Ko, J. Yin and J. Yoon, *Coord. Chem. Rev.*, 2018, **354**, 74–97.
7 L. Yu, X. Fan, H. Zhao, C. Ding, Y. Zhang, J. Fan and X. Tang, *Dyes Pigm.*, 2022, **206**, 110600.

8 W. Wang, A. Fu, J. You, G. Gao, J. Lan and L. Chen, *Tetrahedron*, 2010, **66**, 3695–3701.
9 B. Rathinam, C.-C. Chien, B.-C. Chen and J.-H. Liu, *Tetrahedron*, 2013, **69**, 235–241.
10 B. Ananda Rao, H. Kim and Y.-A. Son, *Sens. Actuators, B*, 2013, **188**, 847–856.
11 P. Yin, Q. Niu, T. Wei, T. Li, Y. Li and Q. Yang, *J. Photochem. Photobiol., A*, 2020, **389**, 112249.
12 P.-P. Zhang, B. Song, Z. Li, J.-J. Zhang, A.-Y. Ni, J. Chen, J. Ni, S. Liu and C. Duan, *J. Mater. Chem. A*, 2021, **9**, 13552–13561.
13 X. Nan, Y. Huyan, H. Li, S. Sun and Y. Xu, *Coord. Chem. Rev.*, 2021, **426**, 213580.
14 R. AbhijnaKrishna and S. Velmathi, *Coord. Chem. Rev.*, 2022, **459**, 214401.
15 X. Xu, L. Yang, D. Song, J. Zhao, Z. Li, Z. Xu, W. Zhang, Y. Huang and S. Zhao, *Org. Electron.*, 2019, **69**, 241–247.
16 P. Wickramsinghe, P. Deokar, P. I. Djurovich, R. Haiges and M. E. Thompson, *J. Photochem. Photobiol., A*, 2019, **374**, 16–21.
17 E. Lima, A. G. Barroso, M. A. Sousa, O. Ferreira, R. E. Boto, J. R. Fernandes, P. Almeida, S. M. Silvestre, A. O. Santos and L. V. Reis, *Eur. J. Med. Chem.*, 2022, **229**, 114071.
18 G. Chinigò, A. Gonzalez-Paredes, A. Gilardino, N. Barbero, C. Barolo, P. Gasco, A. Fiorio Pla and S. Visentin, *Spectrochim. Acta, Part A*, 2022, **271**, 120909.
19 G. Xia and H. Wang, *J. Photochem. Photobiol., C*, 2017, **31**, 84–113.
20 N. Barbero, C. Magistris, J. Park, D. Saccone, P. Quagliotto, R. Buscaino, C. Medana, C. Barolo and G. Viscardi, *Org. Lett.*, 2015, **17**, 3306–3309.
21 A. S. K. I. A. Karpenko, S. Gioria, R. Kreder, I. Shulov, P. Villa, Y. Mély, M. Hibert and D. Bonnet, *Chem. Commun.*, 2015, **51**, 2960–2963.
22 J. He, Y. J. Jo, X. Sun, W. Qiao, J. Ok, T. Kim and Z. Li, *Adv. Funct. Mater.*, 2020, **31**, 2008201.
23 B. Chen, B. Hu, Y. Chen, Z. Lu, Y. Wang, L. Yang and Y. Huang, *Org. Electron.*, 2023, **120**, 106851.
24 M. S. T. Gonçalves, *Chem. Rev.*, 2009, **109**, 190–212.
25 H. N. Kim, Z. Guo, W. Zhu, J. Yoon and H. Tian, *Chem. Soc. Rev.*, 2011, **40**, 79–93.
26 K. Ilina, W. M. MacCuaig, M. Laramie, J. N. Jeouty, L. R. McNally and M. Henary, *Bioconjugate Chem.*, 2020, **31**, 194–213.
27 E. Lima, O. Ferreira, V. S. D. Gomes, A. O. Santos, R. E. Boto, J. R. Fernandes, P. Almeida, S. M. Silvestre and L. V. Reis, *Dyes Pigm.*, 2019, **167**, 98–108.
28 S. H. Kim, S. K. Han, J. J. Kim, S. H. Hwang, C. M. Yoon and S. R. Keum, *Dyes Pigm.*, 1998, **39**, 77–87.
29 D. S. Conceição, D. P. Ferreira, V. C. Graça, C. R. Silva, P. F. Santos and L. F. Vieira Ferreira, *Tetrahedron*, 2015, **71**, 967–976.
30 N. Fu, Y. Chen, J. Fan, G. Wang and S. Lin, *Sens. Actuators, B*, 2014, **203**, 435–443.
31 S. K. Patil and D. Das, *Spectrochim. Acta, Part A*, 2019, **210**, 44–51.
32 Y. Wang, C. Wang, S. Xue, Q. Liang, Z. Li and S. Xu, *RSC Adv.*, 2016, **6**, 6540–6550.
33 C. Li, Q. Li, L. Zhang, Y. Zheng, L. Pan, Z. Ke and B. Li, *Food Ferment. Ind.*, 2020, **46**, 107–113.
34 Z. D. Hill and P. MacCarthy, *J. Chem. Educ.*, 1986, **63**, 162–167.
35 Y. He, J. Mei, M. Zhou, Y. Zhang, Q. Liang, S. Xu and Z. Li, *Inorg. Chem. Commun.*, 2022, **142**, 109592.
36 S. Lee, B. A. Rao and Y.-A. Son, *Sens. Actuators, B*, 2015, **210**, 519–532.
37 K. J. Wallace, M. Gray, Z. Zhong, V. M. Lynch and E. V. Anslyn, *Dalton Trans.*, 2005, **14**, 2436–2441.
38 T. Liu, X. Liu, M. A. Valencia, B. Sui, Y. Zhang and K. D. Belfield, *Eur. J. Org. Chem.*, 2017, **2017**, 3957–3964.
39 M. Ozdemir, *Sens. Actuators, B*, 2017, **249**, 217–228.
40 L. Xiong, J. Ma, Y. Huang, Z. Wang and Z. Lu, *ACS Sens.*, 2017, **2**, 599–605.
41 H. Liu, S. Cui, F. Shi and S. Pu, *Dyes Pigm.*, 2019, **161**, 34–43.